# Evaluating performance of carbon fiber-reinforced pavement with embedded sensors using destructive and non-destructive testing

Monazami, M., Sharma, A., & Gupta, R.

2022

Case Studies in Construction Materials 17 (2022) e01460

Contents lists available at ScienceDirect

Case Studies in Construction Materials

journal homepage: www.elsevier.com/locate/cscm

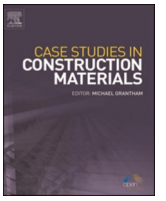

# Evaluating performance of carbon fiber-reinforced pavement with embedded sensors using destructive and non-destructive testing

Maryam Monazami, Ashutosh Sharma, Rishi Gupta *

*Department of Civil Engineering, University of Victoria, Victoria, British Columbia, Canada*

A R T I C L E I N F O

*Keywords:*
Carbon fiber-reinforced concrete
Bus pad
Destructive testing
Sensor-embedded pavement
Non-destructive testing

A B S T R A C T

Installation of concrete pavement at the curb travel lane at the bus stop is a common way to improve the resistance of bus pads to environmental and petroleum deterioration in Canada. The Satisfactory condition of concrete pavements remains a key consideration in the development of infrastructure, especially in countries with an aggressive environment. Innovative materials that could remarkably increase the service life of infrastructure are being researched and developed over decades. This paper aggregates the real-time comparison between the performance of a carbon fiber-reinforced concrete (CFRC) bus pad and a normal concrete bus pad. A series of wireless sensors such as temperature and humidity sensors, thermocouples and strain gauges were embedded in both pavements during the construction. Additionally, a series of six piezoelectric patches were embedded in the concrete in each bus pad. Visual monitoring exhibited that the carbon fiber-reinforced bus-pad remained cracked free while exhibiting some balling of carbon fibers on the surface of pavement whereas the normal concrete bus pads exhibited several hairline cracks in the first 10 days of construction. Along with the visual monitoring using a thermal imaging camera (FLIR), data was acquired regularly from both bus-pads at regular intervals. After 28 days of construction, Non-destructive tests (NDT) including Schmidt Hammer (SH), Electrical Resistivity (ER) and Ultrasonic Pulse Velocity (UPV) were conducted on both the bus pads. When compared to normal concrete bus pads, which have electrical resistivities of roughly 30 kΩ-cm, CFRC bus pads showed extremely low electrical resistivity. Schmidt hammer and UPV both revealed degradation in the normal concrete bus pad in comparison to the CFRC bus pad. Several clusters of very low UPV values were observed in the location of bus pad cracks. The lesser values in the CFRC bus pad are indicative of the scatter in the wave energy due to the presence of carbon fibers.

## 1. Introduction

Infrastructure deterioration is an inevitable process, and aggressive environmental conditions in the entire North American sub-continent proliferate the intensity of degradation. In a 2019 Canadian Infrastructure Report Card developed by the Federal of Canadian Municipalities (FCM), it has been established that long-term investments are urgently required to address the critical infrastructure needs of Canada. Nearly 40 % of roads and bridges are rated as fair, poor, or very poor, and nearly 80 % are over 20 years old [1].

More than 15 million Canadians use public transit such as buses to get to work [2] and an estimate of 142.7 million passenger trips

* Corresponding author.
*E-mail address:* guptar@uvic.ca (R. Gupta).

https://doi.org/10.1016/j.cscm.2022.e01460
Received 29 June 2022; Received in revised form 21 August 2022; Accepted 3 September 2022
Available online 6 September 2022

were recorded in November 2015. Public transit roads are generally developed using asphalt, which is often the most suitable material. Bus stops are subjected to sudden braking and acceleration of buses and asphalt pavement tends to develop waves or ripples (distortion of asphalt) under the weight of the bus (axle loads). As a result, cracks are formed in the asphalt that very often enlarge into potholes. This is usually obviated by constructing bus pads made of concrete to safely accommodate the weight of buses. Concrete Bus Pads (CBP), commonly found at bus stops are the most durable portion of the road surface.

However, concrete's vulnerability and constant exposure to aggressive environments in Canada causes CBPs to deteriorate faster than stated, aggrandizing repair costs [3]. It has been reported that crack width movements are generally larger at the top surface of concrete pavement, and crack width movements vary across the depth due to varying temperatures. Further, it was also suggested that crack width movements increase with a decrease in longitudinal steel ratio [4]. In another study [5], it was found that the geometry of the concrete slab significantly influences the potential for longitudinal cracking, especially when the traffic is composed of more tandem and tridem axles. It has been reported that temperature during the construction and curing of concrete slabs greatly influences the cracking [6]. In general, deterioration in CBPs is related to higher tensile stresses than its tensile strength and is usually due to concrete shrinkage, temperature changes in concrete, traffic loads, low humidity, wind, etc.

Fig. 1 shows the deterioration of the pavement with time. Phase A corresponds to the slow progression of deterioration of the concrete pavement, restricted to the top surface. During this phase, deterioration remains a function of the quality of construction, materials used, design mix, and the routine maintenance regime. This is followed by phase B, wherein deterioration is accelerated and makes inroads across the depth of the concrete pavement. In phase C, the surface of the pavement is completely cracked and damage continues to increase significantly. It should be noted that repair and rehabilitation can only be done until phase C. In phase D, the pavement is significantly damaged. Although the pavement can still last for some more years, it requires replacement for safe transit applications. With each passing phase, the cost of repairs and maintenance also rises exponentially.

The increased service life of the pavement implies that the condition of the pavement should remain in phase A for a longer duration. This can only be done by successfully preventing the microcracks from developing in the concrete. The prime focus of this study is to increase the service life of the bus pad by limiting the cracking during the initial phase and as a result, prolonging phase A of the deterioration curve.

In the last two decades, different kinds of fibers (steel, polypropylene, glass, natural fibers, etc.) have been tested for improving concrete composite's mechanical behavior [8–13]. By the principle of adhesion and mechanical bond, e.g., the anchor effect of interlocked fibers, fibers can improve the mechanical strength characteristics and post-crack toughness of the composite [10]. The randomly oriented fibers have the ability to effectively prevent the extension and propagation of internal micro-cracks when they emerge in concrete. This is known as the fiber bridging effect [14]. Metallic fibers such as steel fibers, etc. significantly improve the mechanical behavior of concrete, but their vulnerability to corrosion, exposure to vehicles due to abrasion of pavement, etc. makes them unsuitable for use [15].

Synthetic fibers obtained from petroleum products are chemically inert and have a much greater modulus than concrete [16]. Different types of synthetic fibers are being explored as construction materials such as Polypropylene (PP) [17–20], Poly Vinyl Alcohol (PVA) [21–24], polyolefin (PO) [25–28], Carbon [29–32], Polythene (PE) [33,34], Polyester [35–39], Acrylic [40–42], Nylon [43–46] and Aramid [47]. Of all the synthetic fibers, polypropylene fibers have been extensively researched and used in concrete. Utilizing polypropylene fiber in fiber concrete technology is recommended to improve mixtures' water resistance, frost resistance, impact strength, and abrasion resistance, as well as to prevent mixture delamination [15]. However, due to their low modulus, they have a moderate influence on the mechanical behavior of concrete. Recently, the potential of carbon fibers for various applications in concrete is being researched and explored. The primary study on carbon fiber concrete composites was conducted in 1973 [48], wherein superior mechanical properties of PAN-based carbon fiber-reinforced concrete composites were reported. Owing to their high modulus, it has been proposed that carbon fibers can significantly reduce plastic shrinkage cracking [29,49], improve thermal resistance, weather ability, and chemical stability in aggressive environments [49]. Although various studies investigated the effect of carbon fibers in concrete, most are limited to laboratory tests, and, to the best knowledge of the authors, there are only few studies that have reported the field applications of carbon fibers especially in concrete bus pads. As a result, in order to gain further insight into the development and field performance of CFRC pavements, a thorough evaluation of the behaviour of pavement is required. It is

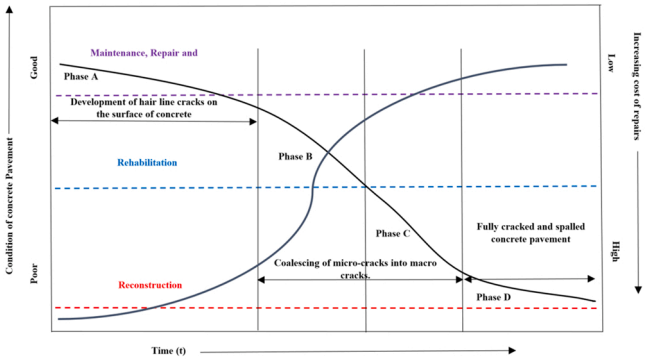


**Fig. 1.** Deterioration of pavement with time [7].

noteworthy to mention that the cost of carbon fiber-reinforced concrete will be higher than conventional concrete mainly due to the cost of the fibers. However, the longer service life, possible reduction in steel can justify part of the added cost. Life cycle assessment of the developed material is being investigated by the authors and will be included in future publications.

In consideration of the time-consuming and costly conventional destructive tests, the use of non-destructive techniques (NDTs) has emerged as one of the main methods of evaluating the post-construction structural performance of roads and pavements. There are several NDT techniques that are currently being employed in the condition assessment field. These techniques include surface hardness methods such as Schmidt hammer [50], resonant frequency tests (by vibration or by impact) [51], maturity methods [52], ultrasonic pulse velocity methods [53], impact echo methods [54] and many more methods that are mainly employed to determine the quality and integrity of concrete without affecting its functions [55]. A set of NDTs is usually operated on the whole pavement in the first phase. After the data interpretation, locations with potential deficiencies will be identified and such points receive a more in-depth study with potential material extraction. The approach used in this research was created to fill a gap in the literature by conducting a number of non-destructive field tests and subsequently analyzing the data to gain a thorough knowledge of carbon-fiber-reinforced pavements with the aim of designing a crack-free concrete bus pad. A set of sensors were used in both pavements to monitor the temperature, humidity, and strain variations and a performance based comparison between the carbon fiber-reinforced concrete bus pad and a normal concrete bus pad have been investigated.

## 2. Materials and methodology

### 2.1. Selection of carbon fibers

Three different fiber types with varying lengths, material characteristics, and sources were obtained during the early phase of this investigation. Mitsubishi Chemicals supplied PAN-based and pitch-based carbon fibers, while Teijin Cooperation supplied another set of PAN-based carbon fibers. Initially, limited quantities of fibers were obtained for testing lab-based mortar and concrete samples. Teijin fibers with longer lengths performed better during the early testing of carbon fiber-based composites. Table 1 shows the physical and chemical properties of the fibers used in the preliminary phase.

#### 2.1.1. Initial testing of carbon fibers based composites

For the construction of the bus pad, initial testing of materials was conducted in the Facility for Innovative Materials and Infrastructure Monitoring (FIMIM) at the University of Victoria with multiple objectives: 1) to select the most suitable carbon fibers; 2) to select the most suitable length of carbon fibers; 3) to select the optimum dosage of carbon fibers. To achieve these objectives, 17 groups of mortar mixtures including cement mortar with different fiber concentrations and lengths were considered, and 6 mix designs were chosen for further investigation in the concrete phase [56]. The design mix for mortar and concrete samples was developed as per ACI 544–1 [57], with a target strength of 32 MPa. The involved properties include flowability, workability, tensile, compressive, and flexural strength. To obtain reliable test data, a minimum of 3 specimens was used to calculate the average. Table 2 entails the details of different types of carbon fiber-reinforced mortar and concrete samples cast, fiber concentrations, fiber length, and the corresponding ASTM standards for the test.

Quikrete General Use (GU) cement conforming to CSA A300 standard [65] was used as the binder. The fineness modulus of fine and coarse aggregates was 2.85 and 7.03 respectively. All samples were cured under ambient conditions and tested after 28 days of curing.

Fig. 2 shows the quadric polynomial fitted surface of compressive strength, tensile strength, flexural strength, and flexural energy absorption of CFRMs. Abbreviations were denoted in such a way that the last number illustrates the length of the fiber. PAM, PIM, and PAT denote samples with PAN-based Mitsubishi carbon fiber, Pitch-based Mitsubishi carbon fiber, and PAN-based Teijin fiber respectively. Considering the maximum points of the surface, the optimized range for compressive, tensile, and flexural strength of CFRMs was shown to be between 0.5% and 1% of fiber content. However, the optimum fiber dosage for energy absorption was observed to be 2–3% of fiber content. The models also approve the positive effect of fiber length on the flexural behavior of samples. Among the investigated CFRMs and CFRCs, samples with 0.5% and 1% fiber content are likely to be more effective because these samples have the highest improvement in most of the investigated mechanical properties compared to normal concrete.

### 2.2. Selection of site

With the help of local authorities at Saanich municipality and BC Transit, a local survey of bus pads in the Saanich municipality was done by the research team. Finally, a site at the University of Victoria bus exchange was identified that included a series of four bus pads. Out of the four bus pads, permission to replace three of them was sought. The plan of the slabs, the construction details of the

**Table 1**
Physical and chemical properties of fibers.

| Type | Source | Length | Filament Diameter | Specific Gravity | Tensile Modulus | Tensile Strength |
|---|---|---|---|---|---|---|
| | | (mm) | (μm) | | (GPa) | (GPa) |
| PAN-based carbon fiber | Mitsubishi | 6 | 6 | 1.8 | 234 | 4.8 |
| Pitch-based carbon fiber | Mitsubishi | 6 | 11 | 2 | 186 | 2.34 |
| PAN-based carbon fiber | Teijin | 6, 12 & 18 | 7 | 1.9 | 227 | 4.89 |

**Table 2**
Preliminary tests on carbon fiber-reinforced mortar (CFRM) and carbon fiber-reinforced concrete (CFRC).

| Type of Composite | Sample Geometry | Sample Dimensions (mm) | Fiber Concentration % (Vol) | Fiber length (mm) | Test | Standard |
|---|---|---|---|---|---|---|
| CFRM | – | – | 0.5, 1, 2, 3 | 6, 12 | Flowability | ASTM C1437 [58] |
| | Cubes | 50 × 50 × 50 | 0.5, 1, 2, 3 | 6, 12 | Compressive strength | ASTM C109 [59] |
| | Dog bones | critical length = 25.4 × 25.4 | 0.5, 1, 2, 3 | 6, 12 | Tensile strength | ASTM C307 [60] |
| | Beams | 30 × 30 × 100 | 0.5, 1, 2, 3 | 6, 12 | Center-point bending | ASTM C293 [61] |
| CFRC | – | – | 0.5, 1, 2 | 6, 18 | Slump flow | ASTM C143 [62] |
| | Cylinders | 100 × 100 × 200 | 0.5, 1, 2 | 6, 18 | Compressive strength | ASTM C39 [63] |
| | Beams | 100 × 100 × 400 | 0.5, 1, 2 | 6, 18 | Center-point bending | ASTM C293 [61] |
| | Circle panels | 800 × 800 × 75 | 0.5, 1, 2 | 6, 18 | Round panel bending | ASTM C1550 [64] |

pavement, and the Google map of the bus pads location are presented in Fig. 3. Abbreviations were denoted in such a way that bus pad #1 is abbreviated to $B_{N\text{-}1}$, bus pad #2 is abbreviated to $B_{N\text{-}2S}$, and bus pad #3 is abbreviated to $B_{CF\text{-}S}$ (letter N, S, CF applies to Normal concrete, Sensor and Carbon Fiber). Fig. 4 shows the deteriorated bus pads selected for this study.

#### 2.2.1. Image analysis on pre-existing bus pads

Before replacing the bus pads, the condition assessment of existing bus pads was conducted. Image analysis was performed using ImageJ software to quantify the antecedent damage in the deteriorated bus pads. Fig. 5 shows the different images of the bus pads that were analyzed to evaluate the total crack area, crack area fraction, maximum crack width, and average crack width for all bus pads were calculated. Table 3 shows detailed results of image analysis of the pavements. It can be seen that bus pad #2 had the worst condition in regard to the highest crack area and bus pad #1 was the worst pavement in regard to the highest average crack width. Further, it should be noted that all the bus pads were in phase D of the 'pavement condition curve'.

### 2.3. Site development

#### 2.3.1. Excavation of the existing bus pads

In order to implement real bus pad construction practices available in Victoria, a local contractor was hired for undertaking all stages of the project including excavation, sub-base compaction, reinforcement installation, concrete mixing, and pouring. Excavation of deteriorated bus pads was done two days before the concrete pouring. According to BC Transit Infrastructure Design Guidelines [66], the concrete bus pad thickness should be designed as follows: 225 mm for portland cement concrete, 150 mm for base coarse, and 300 mm for sub-base coarse. However, the constructed bus pad consisted of a 125-mm thick layer of concrete. Upon excavation, a thin wire mesh was laid on the bed of the pad. Fig. 6 shows the excavated bus pad site.

#### 2.3.2. Installation of sensors

The construction of the bus pads was scheduled two days after the excavation work was completed. This was done primarily for of the installation of different types of sensors. After the excavation was complete, a complete survey of the excavated bus pad was conducted and the actual depth at multiple points was noted (as shown in Fig. 7). Out of the three excavated bus pads, two of them ($B_{N2}$ and $B_{CF}$) were selected for the embedment of sensors. The sensors were installed inside the bus pads with a dual objective: 1) to monitor the deterioration of $B_{N2}$ and $B_{CF}$, with time; 2) to monitor the behavior of the bus pads under different volumes of traffic. To achieve the objectives, a series of wireless temperature and humidity sensors, thermocouples, strain gauges, and piezo patches were installed in the bus pad. Furthermore, an on-site workstation was also developed on the curb wherein all the wires coming from both the bus pads were laid. This was developed to be able to access data at the site while the bus pad was open to traffic. Fig. 7 shows the location of different sensors inside the bus pad. The sensors used are given in the figure and described in the following sub-sections.

*2.3.2.1. Temperature and relative humidity sensors.* A series of BlueRock™ sensors for measuring temperature and relative humidity were procured from Giatec Scientific. These sensors can map the temperature and humidity of in-place concrete from fresh to hardened stages. Using the BlueRock™ mobile app, real-time variations in the concrete's internal humidity can be studied. A total of 5 BlueRock™ sensors were tied to the wire mesh at different locations (as shown in Fig. 8), inside $B_{N\text{-}2S}$ and $B_{CF\text{-}S}$ as well. In addition to BlueRock™ sensors, two thermocouples (Type WENK-01), with a diameter of 0.3 mm were also embedded inside each bus pad for continuous monitoring. A NI-data logger was employed to acquire data from the thermocouples. Fig. 7 shows the details of the location of the sensors.

*2.3.2.2. Strain gauges.* The bus pads were also instrumented with strain gages, deployed in rosettes at different locations. A set of concrete materials using pre-wired strain gauges from Tokyo Sokki Kenkyujo Co. were acquired to monitor the displacement of the slabs. The strain gauges had thin stainless steel backings to avoid the penetration of moisture from the reverse sides. The strain gauges had moisture proofing over-coating and integral lead wire in addition to the stainless steel backing. These strain gauges are intended for long-term measurement of concrete structures, consisting of a 10-mm-long gauge with 118 ± 0.5 Ω gauge resistance. Each strain gauge was wired with a 3-m-long lead wire with a resistance of 0.32 Ω/m. Each strain gauge was mounted on a #3 rebar with a length

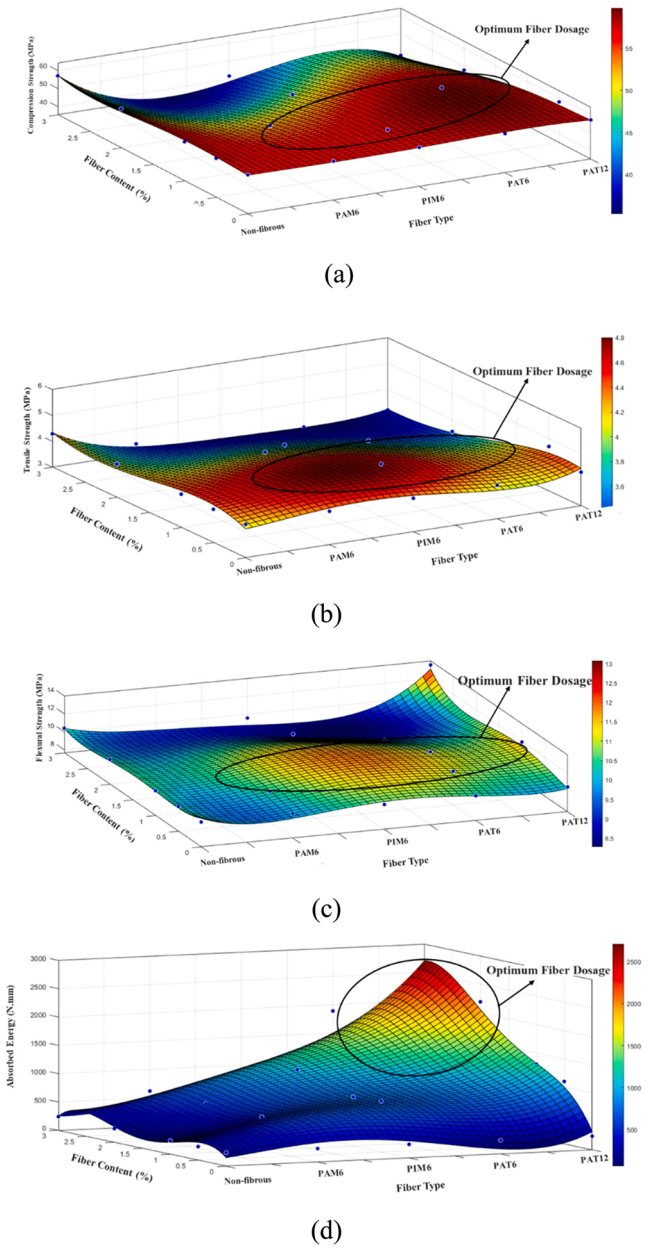


**Fig. 2.** Preliminarily tests results on CFRMs (a) compressive strength (b) tensile strength (c) flexural strength (d) Absorbed energy under flexure [56].

of 100 mm, and the rebar was loosely tied to the embedded wire mesh. The strain gauge had an error in recording thermal strains to the order of $11 \times 10^{-6}$/C. Preliminary frequent visits to the bus pad enabled researchers to find the expected locations of the wheel loads and hence, three strain gauges were installed orthogonally (forming a rosette) at each designated location. This was done to obtain the strains in all directions The detailed location of strain gauges is shown in Fig. 7**.** It should be noted that each thermocouple was deployed close to the strain rosette to enable any required temperature correction. A National Instruments Data Acquisition system (DAQ) was used to read the values of strain gauges. Fig. 8 Shows the details regarding the installation of strain gauges and BlueRock™ sensor.

*2.3.2.3. Piezoelectric patches.* A piezoelectric patch is a thin flexible commercially manufactured piezo ceramic transducer that works on the principle of converting electrical signals to stress waves and vice-versa. When a high input voltage is applied to a piezoelectric patch, it creates a mechanical strain that excites the host structure. A piezoelectric patch that generates stress waves within a host structure is called an 'actuator', and the patch that receives these stress waves is called a 'sensor'. Piezoelectric patches can be

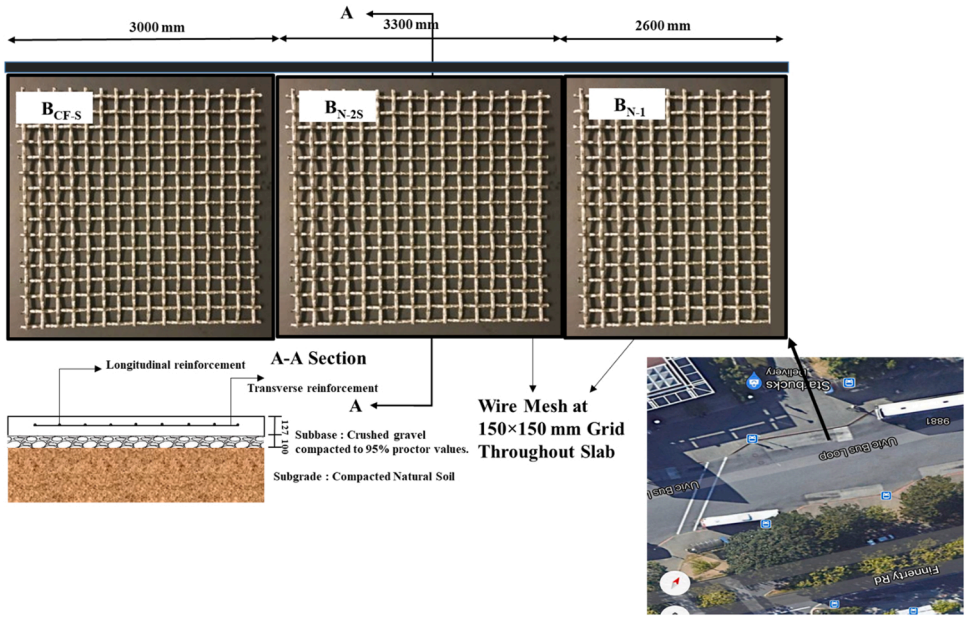


**Fig. 3.** Details of the pavement and the construction site.


**Fig. 4.** Pre-existed condition of bus pads (a) $B_{N-1}$ (b) $B_{N-2S}$ (c) $B_{CF-S}$.

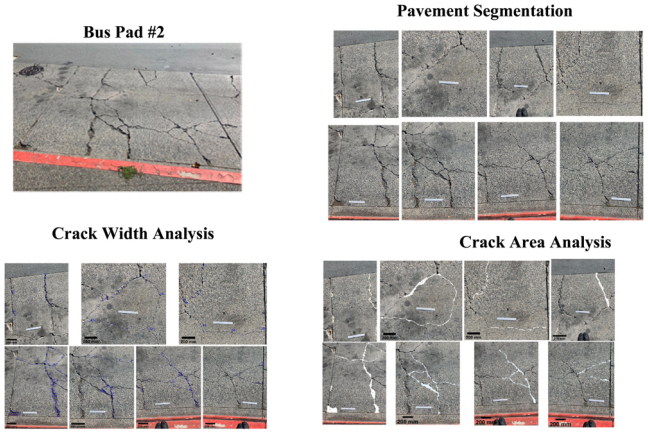


**Fig. 5.** Image Analysis of pre-existing bus pad.

**Table 3**
Crack Analysis of existing bus pads.

| Code | Crack Area ($mm^2$) | Crack Area/Pavement Area (%) | Maximum Crack Width (mm) | Average Crack Width (mm) |
|---|---|---|---|---|
| $B_{N-1}$ | 150246 | 2.33 | 253 | 35.53 |
| $B_{N-2S}$ | 301796 | 3.05 | 219 | 14.41 |
| $B_{CF-S}$ | 101203 | 1.12 | 65 | 17.70 |

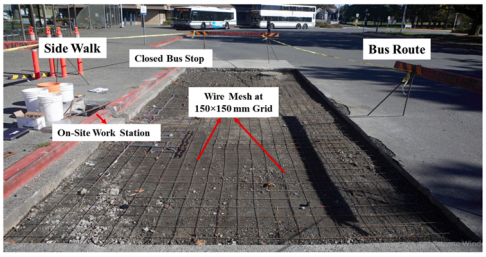


**Fig. 6.** Excavated bus pad site.

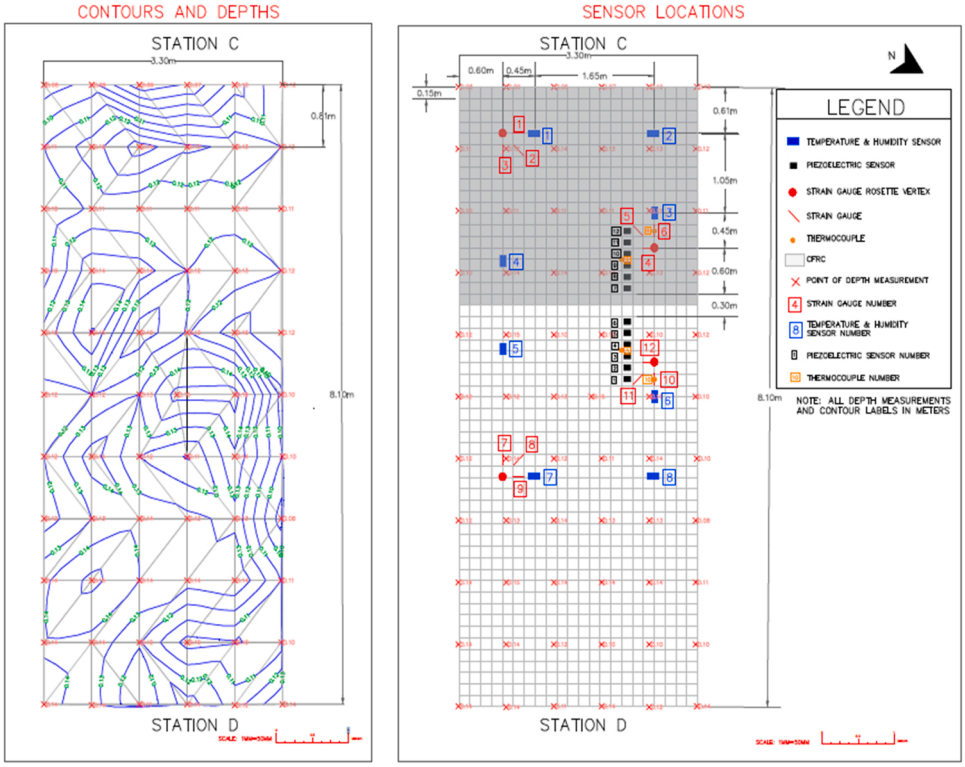


**Fig. 7.** The layout of bus pads and sensor location.

embedded in a concrete structure for early detection of damage by evaluating various phenomena occurring within the concrete.

In order to further quantify the behavior of bus pads subjected to aggressive environmental conditions in addition to the busloads, monitoring of bus pads using piezoelectric patches was also implemented. Two sets of piezoelectric patches were embedded in an array form in $B_{N-2S}$ and $B_{CF-S}$, as shown in Fig. 9. An array of 6 piezoelectric patches were embedded in $B_{N-2S}$ with a spacing of 150 mm between consecutive patches. At a gap of 300 mm from the last piezoelectric patch in $B_{N-2S}$, another array of 6 piezoelectric patches with the same spacing were embedded in $B_{CF-S}$. The piezoelectric patches were secured with tape to the grid to hold them in the correct location when the concrete was poured. The wires from the electrical contacts of piezoelectric patches were secured to the grid, protected by transparent ducts, and guided through the curb to the separate compartments. These compartments, as shown in Fig. 9,

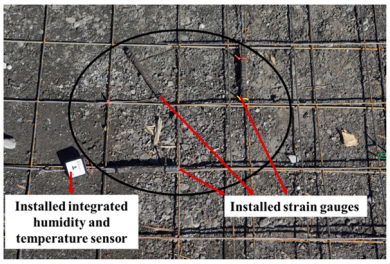


**Fig. 8.** Installed sensors and strain gauges.

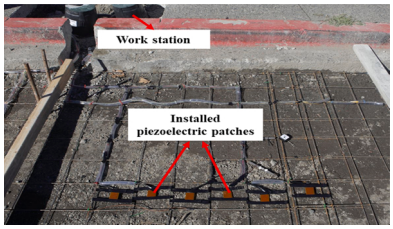


**Fig. 9.** Installed piezoelectric patches.

installed within the sidewalk allowed the monitoring of $B_{N\text{-}2S}$ and $B_{CF\text{-}S}$ over time. The concrete signatures recorded by piezoelectric sensors at different time intervals can be linked with induced damage such as progressive cracking. It should be noted that the study using Piezo patches is still ongoing and will be reported in the subsequent papers.

### *2.4. Design mix and placing of concrete*

The estimated amount of concrete required for three bus pads and several molds for lab testing of concrete was more than 6 cubic meters and therefore, the concrete was supplied by a local ready-mix concrete producer. A local contractor was hired to bring a truck of dry concrete to the site. The concrete ordered had a target strength of 30 MPa and an air content of 5–8 %. The maximum size of aggregates used was 12 mm and a slump of 80 mm was desired. It should be noted that properties of fresh concrete such as slump value, air content, bulk density, etc. were evaluated on-site as per ASTM C143 [62] and ASTM C231 [67] at the time of construction of bus pads.

In a truck mixer with a capacity of 10 $m^3$, dry concrete was mixed with water at a w/c ratio of 0.5. The appropriate amount of CF was packaged in 5 kg water-soluble bags. The concrete mixing and placing procedure followed in the concrete plant and at the job site was as follows:

1- A few hours before concrete pouring, the sensors were cleaned, and their connectivity to the work station was checked.

2- With the arrival of the drum mixer, quality control on concrete including two sets of slump test and air meter test was operated. The weather temperature was reported to be 10°C.

3- The normal concrete was poured in the first 2 slabs, spread manually, consolidated by a vibrating screed, and finished. Six 100 × 100 × 200 mm cylinders, six 100 × 100 × 400 mm beams, two 75 × 75 × 800 mm panels were taken from the plain concrete in the field. Then the mixer was stopped.

4- The fibers were incrementally added to the concrete truck. Considering the optimum amount of 0.5 %– 1 % from the

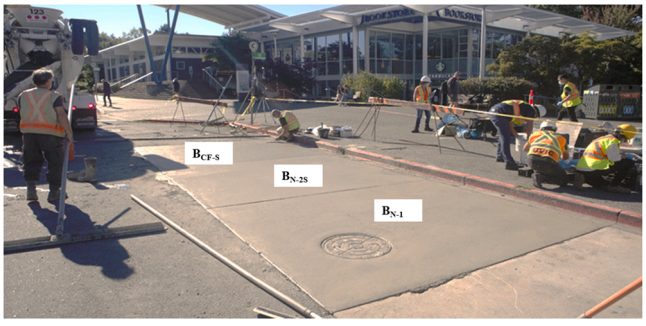


**Fig. 10.** Finished bus pads.

experimental results, and by calculation of the amount of poured concrete, a sufficient amount of carbon fiber was added to the mixer in order to meet the targeted fiber dosage. The volume of fiber added into the concrete turned out to be 0.55 % which is in accordance with the optimum experimentally obtained dosage. In order to assess the uniform dispersion of fibers in concrete, three cylinders were filled with fresh CFRC and were taken to the laboratory for further investigation. The concrete was washed away and fibers were sieved from cement paste. The fibers were then oven-dried and weighed. A fiber volume fraction of $V_f = 0.58$ %, 0.54 % and 0.59 % was calculated from each cylinder. This confirmed the approximate uniform distribution of carbon fibers over the entire bus pad.

5- A carbon-fiber-reinforced bus pad was then screeded and finished. It should be noted that during the screeding of $B_{CF\text{-}S}$, agglomerated fibers were found on the surface of the slab. Fig. 10 shows the finished bus pads constructed with normal concrete and carbon fiber-reinforced concrete.

## 3. Results and discussions

### 3.1. Laboratory-based tests on concrete

#### 3.1.1. Destructive tests (DT)

In order to evaluate the quality of concrete placed at the site for the construction of bus pads, 6 beams, 6 cubes, 6 cylinders, and 2 round panels for each mix were cast and cured for 28 days. Table 4 gives the details of the samples. It should be noted that samples were subjected to dry curing at ambient temperature to simulate the real conditions experienced at the bus pad site in the laboratory. Later, the samples were tested under compression using a compressive testing machine. The average 28-day compressive strength obtained for cylinders made with normal concrete was 20 MPa and for those of carbon fiber-reinforced concrete cylinders was 18 MPa (loss of 15 %). The results indicate that the addition of fibers slightly decreased the compressive strength of concrete mainly due to the workability reduction. Considering the preliminary tests, the reduction rate in bus pad samples is in good correlation from those obtained in the lab, wherein a decrease up to 16 % in compressive strength was seen at 0.5 % fiber volume.

The peak load, its corresponding displacement, the Modulus of Rupture (MOR), pre-crack/post-crack flexural toughness, and the absorbed energy at certain deflection (2.5 mm and 5 mm) of beams and round panels were obtained through the load-displacement curve. The detailed results are presented in Table 4. According to the results, the influence of the incorporation of carbon fibers on the flexural behavior of concrete is more distinct than on compressive strength. A 26 % increase in flexural strength of CFRC beams was observed during flexural testing, while the improvement in the round panel was negligible. The strength improvement in beams is mainly due to the confinement ability of carbon fibers in flexure, holding, and bridging microcracks and as a result, retarding the initiation and growth of cracks and compensating the strength reduction caused by low workability. However, the difference between the results of beams and round panels is mainly due to the different methodology used in the two tests. In the center-point bending test, the specimens are forced to crack at a given location, hence the crack does not necessarily open at the section with low strength material. However, when round panels are subjected to bending, yield lines follow the weakest sections. In concrete panels reinforced with 18 mm fibers, it is hard to avoid fiber balling and get uniform distribution throughout the concrete mix and as a result, the weak section cab is either at the location of fiber balling or at the location where the fiber reinforcement is not sufficient, hence showing a similar MOR compared to CO.

Fig. 11 compares the post-crack energy absorption of samples. It should be noted that although the peak load for CFRC beam samples is reported to be greater than that of the CO beams, there is minimal improvement in the post-crack behavior of the beams while the red area (post-crack absorbed energy) is quite large in round panels. The obtained results are mainly owed to the fact that larger fracture areas, with a much higher number of fibers, are involved in round panel testing, and therefore, the behavior of the structure is highly dependent on the material properties including the crack bridging effect of carbon fiber.

### 3.2. Structural health monitoring of bus pads

Using several NDT techniques, the performance of the pavements was monitored from the first hours to 28 days after concrete placement. Fig. 12 shows the non-destructive techniques applied in this study.

#### 3.2.1. Visual monitoring of bus pads

After construction, the bus pads were closed to traffic for 7 days to allow the concrete to gain strength. The research team regularly monitored the constructed bus pads for any sign of cracking. After the bus pad was opened to traffic, the research team conducted visual monitoring twice a day and a FLIR camera was used to monitor the temperature variation at different locations. This was done to

**Table 4**
Summary of flexural behavior of beams and round panels.

| Sample geometry | Label | Peak load | δpeak | δmax | MOR | Energy (J) | | | |
|---|---|---|---|---|---|---|---|---|---|
| | | (N) | (mm) | (mm) | (N.mm) | δ = 2.5 mm | δ = 5 mm | Pre-crack | Post-crack |
| Beam | CO | 6938 | 1.27 | 1.65 | 3.64 | 2.8 | 2.8 | 2.65 | 0.14 |
| | CFRC | 8750 | 2.13 | 5.5 | 4.59 | 5.61 | 6.07 | 4.97 | 1.11 |
| Round panel | CO | 20774 | 2.14 | 2.4 | 4.00 | 24.61 | 24.61 | 23.23 | 1.38 |
| | CFRC | 21000 | 2.7 | 5.1 | 4.04 | 22.85 | 40.04 | 26.53 | 13.51 |

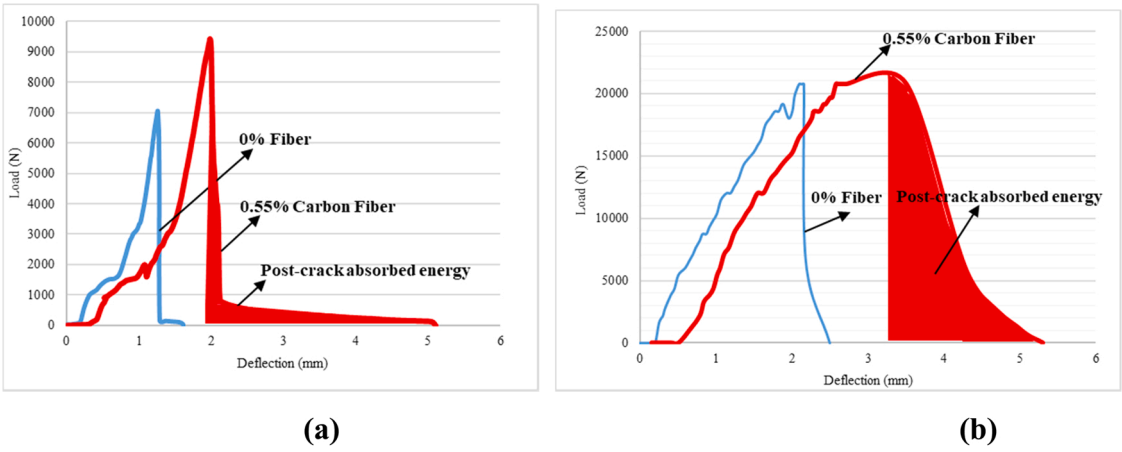


**Fig. 11.** Load-displacement behavior of CO and CFRC under flexure (a) beams (b) round panel.

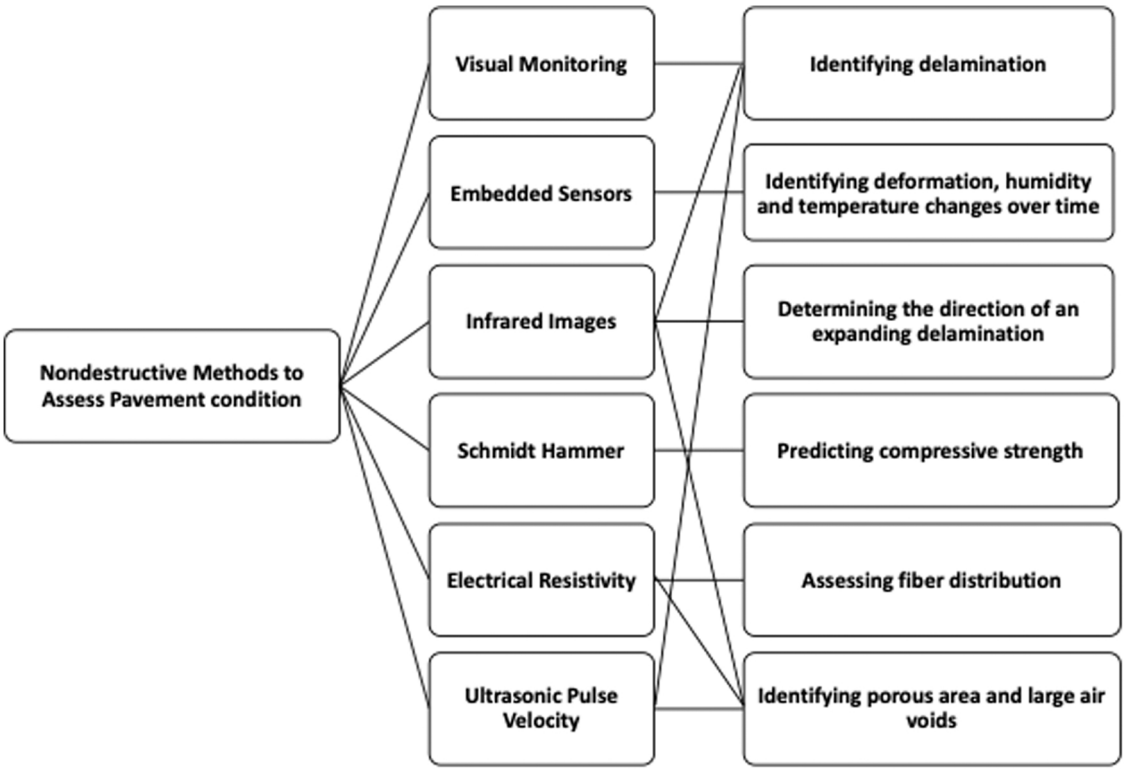


**Fig. 12.** NDTs used to assess pavement condition.

find the potential locations of crack initiation and to track the development of cracks or any other signs of deterioration in the bus pads. Initially, in $B_{CF\text{-}S}$ bus pad, small chunks of agglomerated carbon fibers beneath the top layer of concrete were visible at some. Once the bus pad was opened, it was found that fibers from these areas started coming out due to the abrasion of the surface. However, no cracks were observed in the $B_{CF\text{-}S}$ bus pad. On the contrary, both $B_{N\text{-}1}$ and $B_{N\text{-}2S}$ started developing very thin hairline cracks immediately 7 days after casting. The first cracks which initiated in the middle of the slab is mainly attributed to the combined loading and curling effects and therefore the midspan experienced the maximum deflection [68]. Fig. 13 shows the condition of three bus pads after 28 days of construction. It can be observed that cracks have only slightly widened after 28 days of casting. Thermal imaging photos (using FLIR camera) of $B_{C\text{-}1}$, $B_{C\text{-}2S}$, and $B_{CF\text{-}S}$ are presented in Fig. 14. In the figure, it is easy to see the delaminated areas (lower temperature on the cracks) and the temperature gradient on the pavement which make it possible to determine the direction of an expanding delaminated region [69]. It was also observed that the CFRC bus pad had a uniform temperature variation with a slightly lower internal

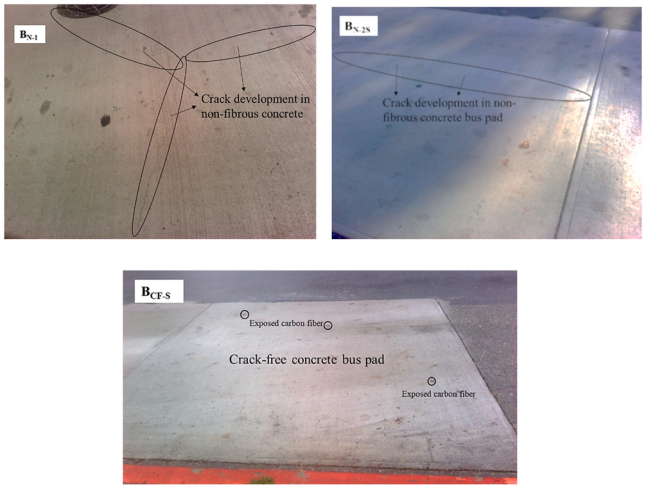


**Fig. 13.** Condition assessment of bus pads at 28 days.

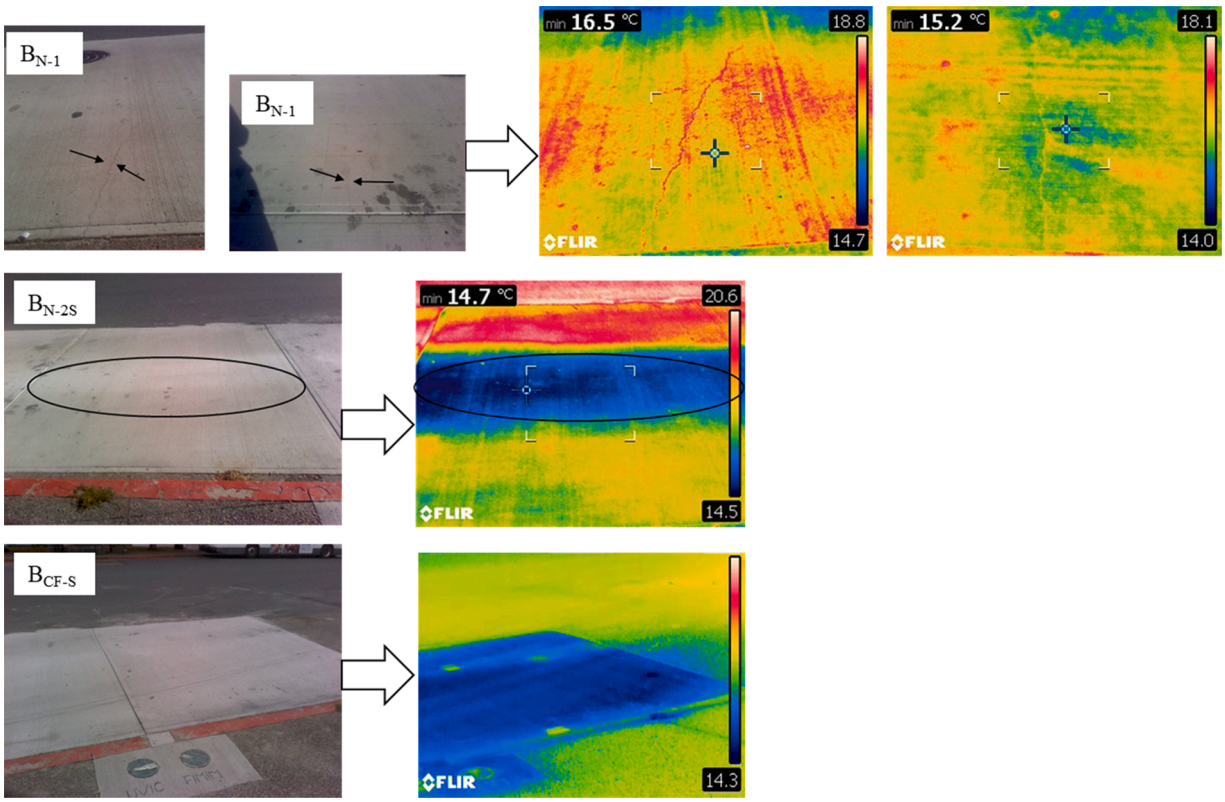


**Fig. 14.** Thermal photos of bus pads.

temperature compared to the other bus pads which is mainly due to the high electrical conductivity of the fibers.

### *3.2.2. Temperature and humidity monitoring of bus pads*

Monitoring the temperature and humidity of concrete provides useful information about the strength gain and maturity of concrete as well as the progress of deterioration mechanisms in the structure. Temperature and humidity data were logged from wireless sensors every eight hours. The logged data was stored on the sensors automatically which was downloaded every day via Bluetooth through the BlueRock™ app. After the construction was completed, the data was logged immediately, and it was found that the wireless sensors embedded in the $B_{CF-S}$ were not able to transmit the data via Bluetooth. This can most probably be attributed to the interference in the

Bluetooth signal by the presence of carbon fibers in the matrix. Fortunately, the thermocouples that were installed for providing temperature corrections to the strain gauge readings were able to record any temperature changes inside the concrete. Fig. 15 shows the variation of data obtained from temperature sensors that were embedded in $B_{N\text{-}2S}$. From the graphs, it can be seen that the temperature variation (based on data from sensors and thermocouples) for the first 30 days in $B_{N\text{-}2S}$ is similar to $B_{CF\text{-}S}$. Temperature variation is primarily a function of the process of hydration, inside the concrete. Additionally, the rate of moisture evaporation which leads to shrinkage and therefore shrinkage strains, inducing cracking in concrete, is a function of air temperature, relative humidity, concrete temperature, and wind velocity [43]. Fig. 15 also represents the variation of temperature based on the data obtained from thermocouples embedded in $B_{CF\text{-}S}$. From the graphs, it can be seen that the trends of temperature change with time are identical for both the normal concrete bus pad ($B_{N\text{-}2S}$) and carbon-fiber-reinforced concrete bus pad ($B_{CF\text{-}S}$). It should be noted that the temperature variation exhibited in both the bus pads is in coherence with the standard temperature variation for concrete. Since embedded BlueRock™ sensors in the $B_{CF\text{-}S}$ bus pad did not work, the humidity-based data is not discussed in this paper.

### *3.2.3. Strain gauge measurements of bus pads*

Initial strain results can be viewed in Fig. 16. It can be observed that the graphs do not conform to a distinct trend. Rather than fluctuating within a limited range, the values appear to primarily consist of what would be considered outliers, readings exceeding the expected limits for strain measured in experimental work, typically − 0.005 to + 0.005 [70]. The strain readings additionally do not conform to either compressive or tensile values, but rather fluctuate between the two strain types. This pattern is observed in gauges 1, 5, 6, 9, 10, 11 and 12, and is therefore not specific to one concrete type. Further investigation will be conducted to determine the cause

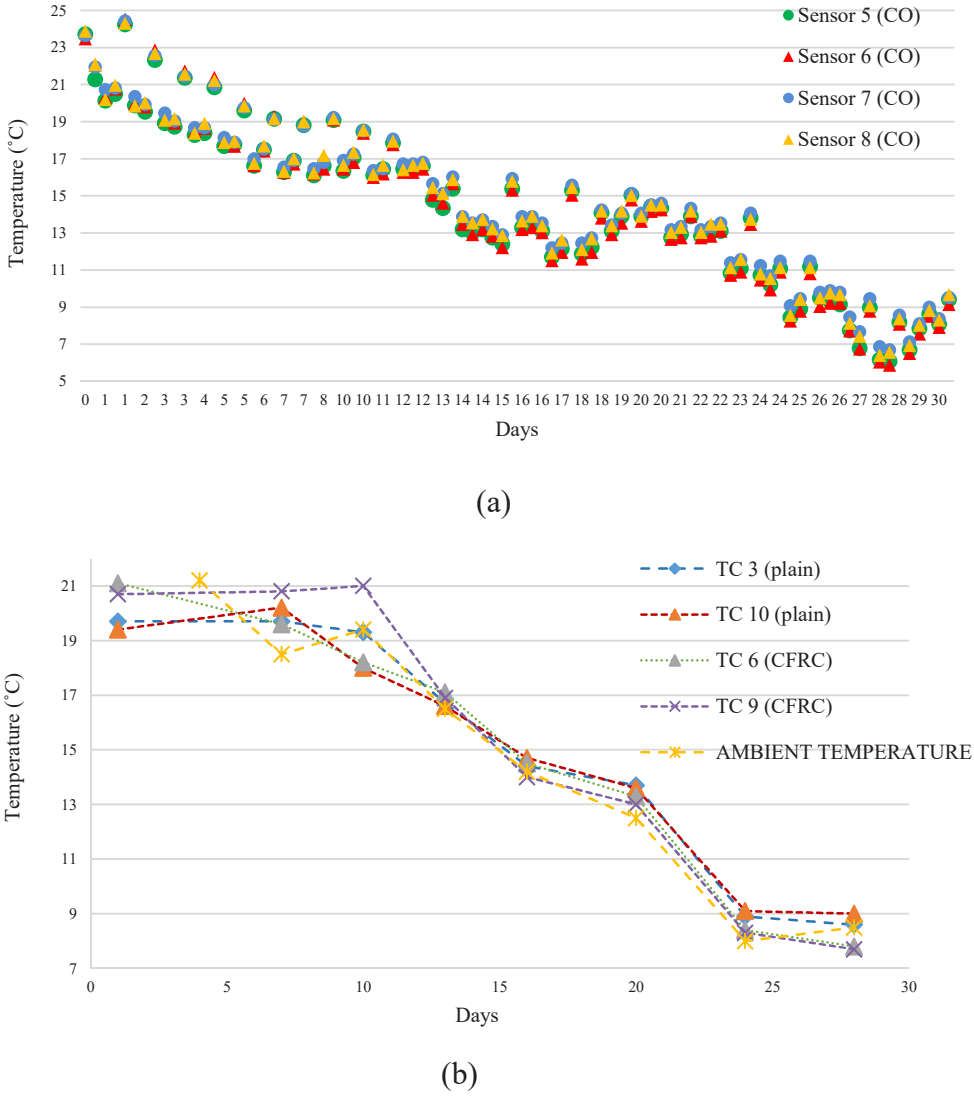


**Fig. 15.** Temperature variation from (a) wireless sensors (b) thermocouples.

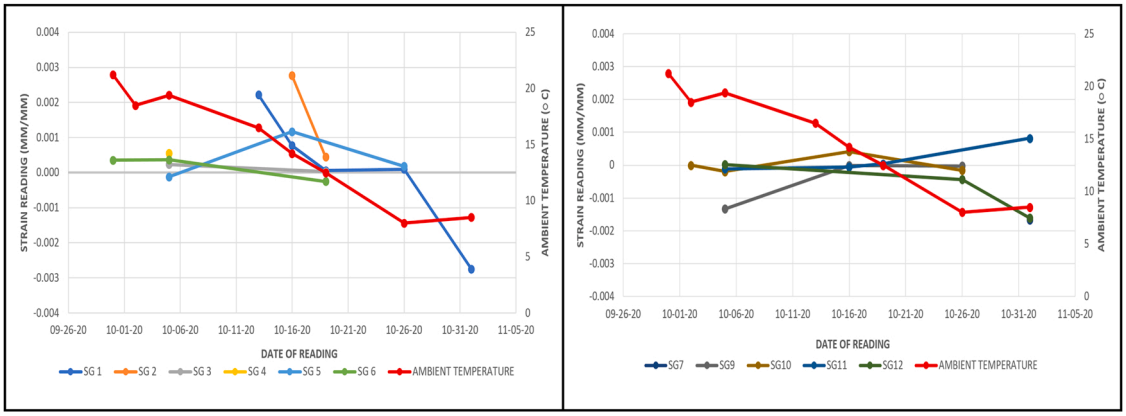


**Fig. 16.** Strain gauge data after temperature corrections.

of inconsistent compression and tension values, as the gauges would be expected to record either only tension or compression only based on their positions in the slab.

### 3.2.4. *Health monitoring of bus pads at 28 days of casting*

After 28 days of construction, permission was granted from BC Transit to close the bus pad to traffic for 5 days, to conduct testing. In addition to regular temperature, humidity, strain gauge, and piezo measurements, three more tests were conducted including Schmidt hammer, Electrical Resistivity (ER), and Ultrasonic Pulse Velocity (UPV) tests. Fig. 17 shows how the gridlines were drawn on concrete bus pads for NDTs.

*3.2.4.1. Schmidt hammer testing.* A rebound hammer is a low-cost method employed to assess the quality of concrete near the surface and to estimate the strength of concrete based on the rebound number. As the rebound hammer test can evaluate the condition of concrete up to a depth of 3 cm effectively [71], it was expected that the rebound hammer test would be able to provide valuable insights.

To evaluate the condition of the bus pad subjected to traffic load, an N-type Schmidt hammer test was conducted as per ASTM C805 [72] for all the bus pads. The three bus pads were divided into grids of 50 cm × 50 cm for the rebound number test and 25 cm × 25 cm for UPV and electrical resistivity tests. The calibration of the rebound hammer was done on an anvil before and after testing. The rebound hammer values were then converted into the corresponding compressive strength values using the chart provided by the manufacturer. The values of compressive strength at different impact points taken by rebound hammer are plotted in Fig. 18. It can be observed that in $B_{N\text{-}1}$ and $B_{N\text{-}2S}$, the average compressive strength is 24 MPa, and for the CFRC bus pad, the average compressive strength is equal to 21 MPa. It should be noted that the rebound hammer predicted compressive strength is in good correlation with those of the samples tested in the lab. It was also observed that the strength values in the center of each slab are higher compared to the concrete placed at the corners. The rebound hammer values were successfully able to differentiate between the material characteristic of plain concrete and fiber-reinforced concrete. The addition of the fibers to the concrete does increase its porosity at this largely affects its surface hardness and hence, impacts the rebound hammer values.

*3.2.4.2. Electrical resistivity.* In general, there are three phases of plain concrete at 28 days [30]: 1) liquid phase with pores containing solutions of water; 2) solid phase including cementitious products of hydration and aggregates; 3) vapor phase with pores filled with air. Both the solid phase and vapor phase have high values of electrical resistivity ranging from $10^{11}$ Ω-cm to $10^{19}$ Ω-cm and hence they act as insulators. The liquid phase has considerably lower values of resistivity of the order of 5–100 Ω-cm and therefore acts as the conductors. Overall, the plain concrete is not electrically conductive with the electrical resistivity of oven-dried concrete at around $10^5$ Ω-cm [31]. Several correlations have been reported that confirm the relationship between the transport parameters of concrete and the durability of concrete. Ion transport through the concrete microstructure controls the durability of concrete. This highlights the importance of electrical resistivity as it defines the ability of concrete to withstand the transport of charged ions in its microstructure. Therefore, the electrical resistivity data can signify the vulnerability of concrete to deterioration as lower values will indicate the easy transfer of ions, which in turn increases the risk of corrosion of the embedded rebar.

The electrical resistivity evaluation of the bus pad utilized the Wenner probe technique, with four equally spaced linear electrodes. All the bus pads were divided into grids of size 25 cm × 25 cm. Readings were taken on the same day (within one hour) to ensure the moisture condition of all slabs was consistent. The electrical resistivity was measured and plotted as a map presented in Fig. 19. From the figure, it can be seen that in the $B_{N\text{-}1}$ and $B_{N\text{-}2S}$ bus pads, electrical resistivity ranges up to 30 kΩ-cm. This confirms the existence of the liquid phase inside the concrete as the testing was conducted only 28 days after construction. The electrical resistivity map also confirms the effect of cracks (presented as zone 1, 2, 3, 4, 5, and 6 on the map) on the resistivity of concrete as the resistivity value is much lower in these areas compared to areas with no cracks.

On the other hand, the electrical resistivity values for the carbon fiber-reinforced concrete were negligible. As carbon fibers are

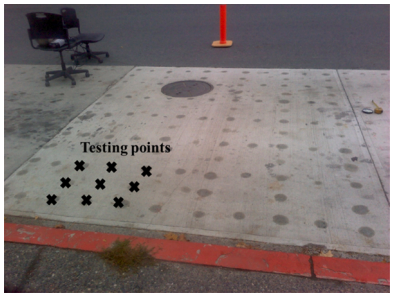


**Fig. 17.** NDT at 25 cm × 25 cm grids on bus pad.

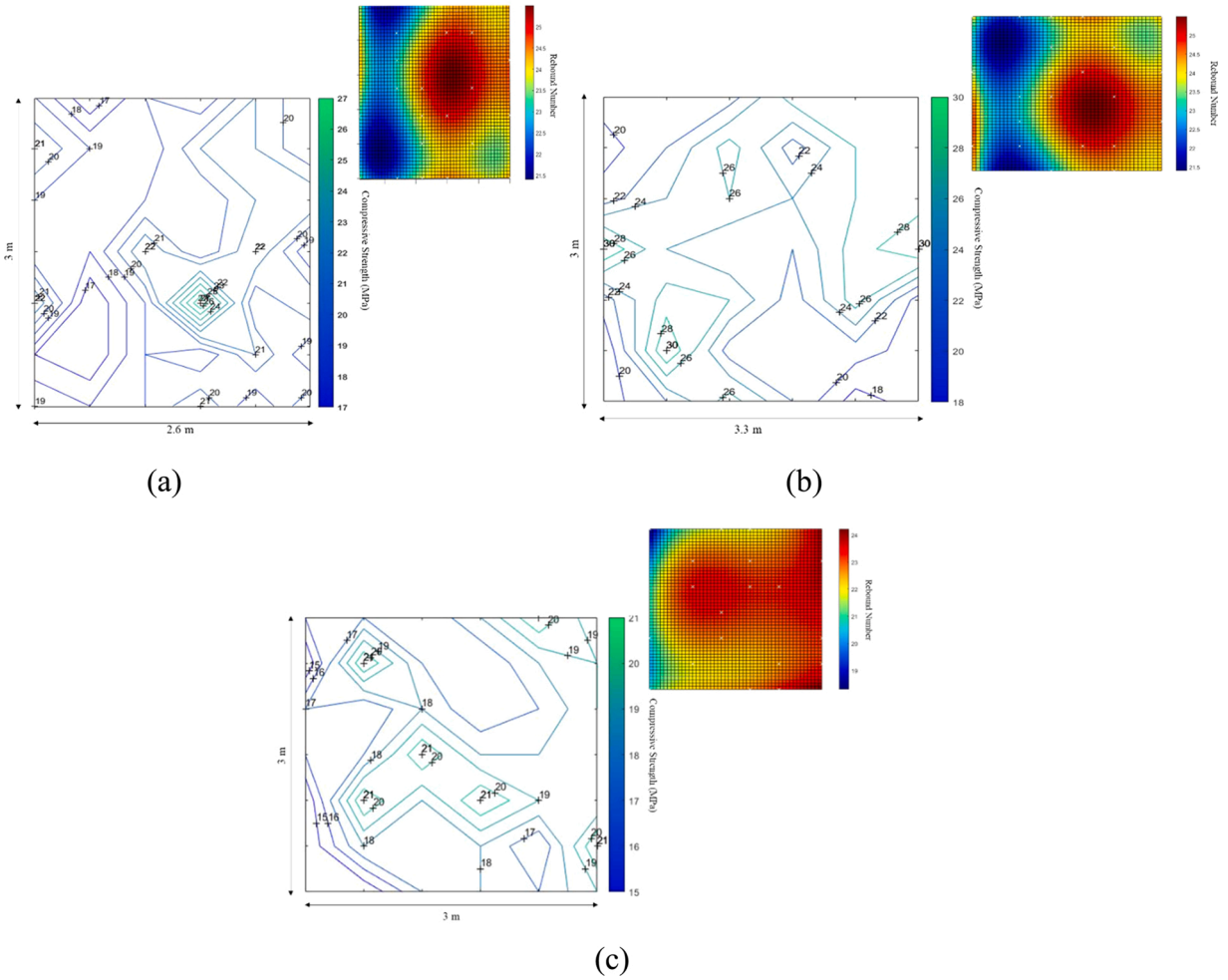


**Fig. 18.** Variation of the Rebound number and compressive strength of bus pads (a) $B_{N\text{-}1}$ (b) $B_{N\text{-}2S}$ (c) $B_{CF\text{-}S}$.

electrically conductive, they significantly reduce the electrical resistivity of the overall composite [73–75]. The uniform low value of electrical resistivity is attributable to the acceptable fiber network formation in the pavement. This further suggests that the measurement of electrical resistivity is not a suitable measure of durability for carbon fiber-reinforced concrete. Fig. 19 also confirms the uniform distribution of carbon fibers in the bus pad as the recorded values of electrical resistivity at all points were nearly negligible. However, this also indicates the effectiveness of a small $V_f$ in reducing the resistivity of a CFRC slab, which could be useful in the future in designing self-sensing properties of CFRC.

*3.2.4.3. Ultrasonic pulse velocity testing.* Elastic waves in concrete are generally influenced by their mechanical characteristics, and

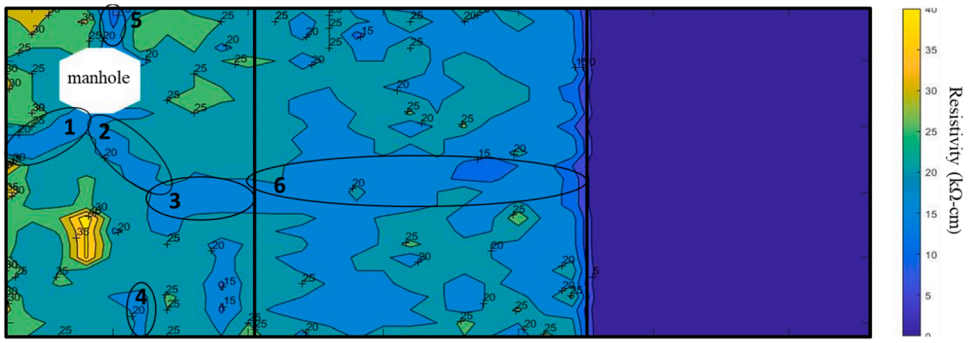


**Fig. 19.** Variation of the Electrical resistivity of concrete across the bus pad (a) $B_{N\text{-}1}$ (b) $B_{N\text{-}2S}$ (c) $B_{CF\text{-}S}$.

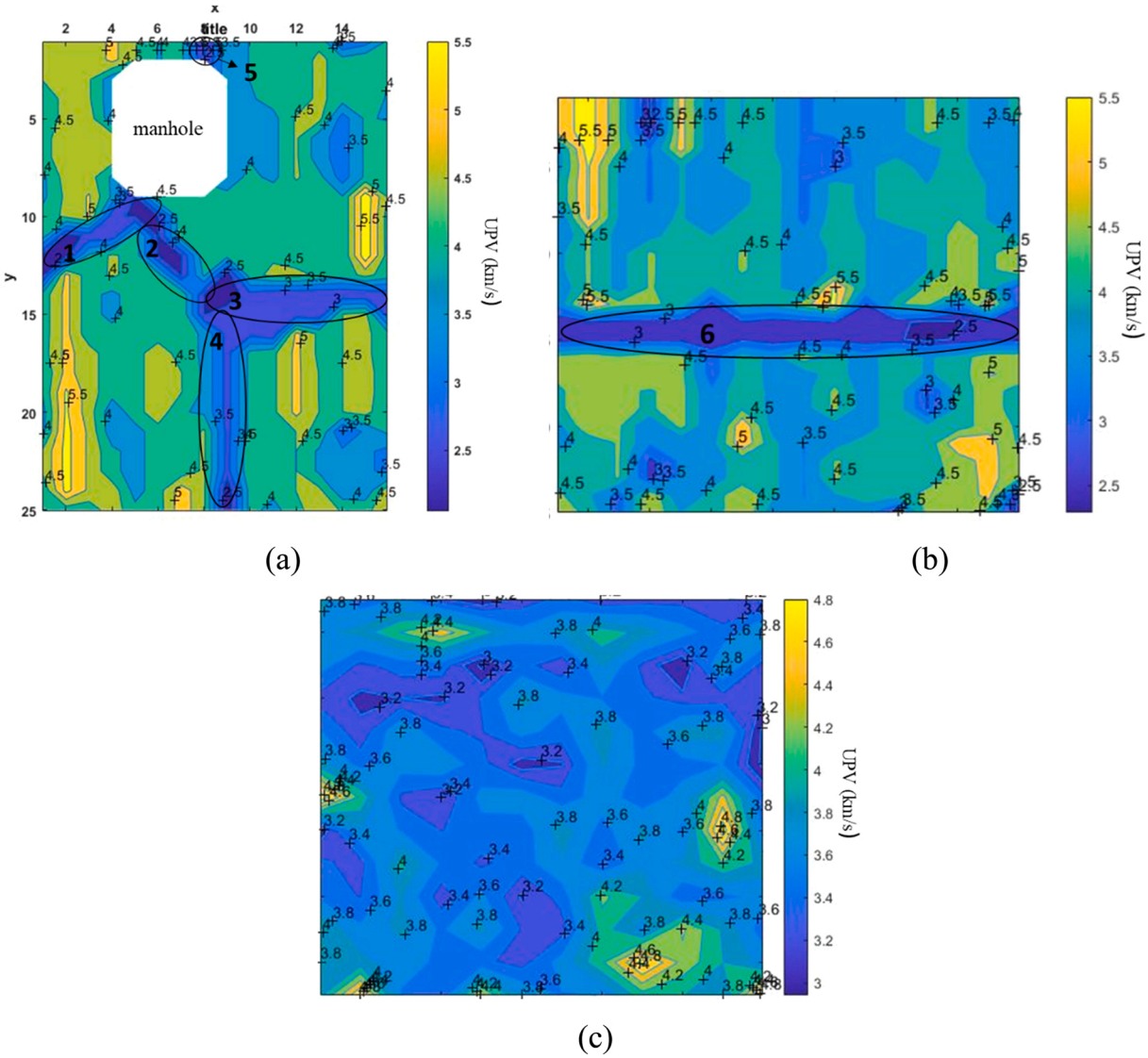


**Fig. 20.** Variation of the UPV of concrete across the bus pad (a) $B_{N\text{-}1}$ (b) $B_{N\text{-}2S}$ (c) $B_{CF\text{-}S}$.

ultrasonic pulse velocity utilizes this principle to estimate elastic stiffness and other strength-related properties. In any material, ultrasonic waves depend on the density of the material and other elastic properties. Hence, for a material such as concrete with a known density, well-defined ultrasonic signals can be used to estimate the modulus of the concrete and also estimate the strength of the concrete.

For testing the concrete bus pads, the Proceq Pundit Lab UPV test instrument was used, with transducers of diameter 50 mm with a maximum frequency of 54 kHz. The UPV testing was conducted as per ASTM- C597–02 [76]. All bus pads were divided into grids of size 25 cm × 25 cm. This implies that the maximum distance between each transducer was 25 cm. All of the acquired data was plotted as shown in Fig. 20. Several clusters of very low wave velocities can be seen in both $B_{N-1}$ and $B_{N-2S}$, marked as zone 1, 2, 3, 4, 5, and 6 in Fig. 20. It should be noted that the marked zones represent cracked areas in the bus pad as observed during the visual inspection of the pads (Fig. 13). For both the $B_{N-2S}$ and $B_{CF-S}$ bus pads, the UPV values vary from 3 to 4.5 km/sec which indicates a good quality of concrete. The inclusion of fibers reduced the rate of UPV penetration into the mixtures, which is consistent with literatures [77,78]. The lesser values in $B_{CF-S}$ also indicate the scatter in the wave energy due to the presence of carbon fibers. Further, the wave velocity is somewhat constant for the entire bus pad, which also indicates good fiber dispersion in the $B_{CF-S}$ bus pad.

## 4. Conclusions

This paper employs the real-time evaluation of carbon fiber reinforced concrete for the purpose of its usage in the construction of a bus pad. Further, the bus pads were equipped with several sensing modules such as temperature sensors, thermocouples, strain gauges, and piezo patches. The data from these embedded sensors were regularly acquired and monitored. In addition to that, several other NDT techniques were employed at 28 days after construction of the bus pad such as Schmidt hammer, electrical resistivity, and ultrasonic pulse velocity. The following conclusions are drawn from the entire study:

1) According to the DT performed on concrete beams and round panels, the influence of the incorporation of CF on the flexural behavior of concrete is reported to be more distinct when compared to the compressive strength. Samples with 0.5 % and 1 % fiber content among the examined CFRMs and CFRCs are more efficient since they exhibit the greatest improvements in most of the mechanical parameters compared to conventional concrete. According to the quadric polynomial fitted surface models, it has been demonstrated that the best fiber dosage for absorbing energy is between 2 % and 3 % of the total fiber content.
2) Flexural testing on sample taken from the site revealed a 26 % increase in the flexural strength of CFRC beams, compared to a negligible improvement in the round panel. Carbon fibers' capacity to retain and bridge microcracks in flexure, which delays the initiation and propagation of cracks is primarily responsible for the strength improvement in beams.
3) During visual observation, in the $B_{CF-S}$ bus pad, small chunks of exposed CF were visible, and it was found that fibers from these areas started coming out due to the abrasion of the surface of the bus pad. However, no cracks were observed in the $B_{CF-S}$ bus pad, while both $B_{N-1}$ and $B_{N-2S}$ developed very thin hairline cracks in the middle of the slab mainly due to the combined stress and curling effects.
4) From the graphs derived from the thermocouples, it can be seen that the trends of temperature change with time were the same for $B_{N-2S}$ and $B_{CF-S}$, and the temperature variation exhibited in both the bus pads is identical and in coherence with the standard temperature variation for concrete.
5) According to the Schmidt hammer test results, the average values for compressive strength were reported to be 24 MPa for $B_{N-1}$ and $B_{N-2S}$ and 21 MPa for $B_{CF-S}$. It was also found that the strength values in the middle were higher than those in the corners. It should be noted that the rebound hammer predicted compressive strength is in a good correlation with those of the samples tested in the lab.
6) The value of electrical resistivity in $B_{N-1}$ and $B_{N-2S}$ ranges up to 30 kΩ-cm, which confirms the existence of the liquid phase inside the concrete as the testing was conducted only 28 days after construction. The electrical resistivity values for the $B_{CF-S}$ were negligible. CF is electrically conductive and the addition of CF in concrete significantly reduces the electrical resistivity of the overall composite. According to the results, the electrical resistivity of $B_{CF-S}$ has a uniformly low value, which can be attributed to the pavement's acceptable formation of a fiber network and an acceptable fiber distribution.
7) Several clusters of very low UPV values were observed in the location of bus pad cracks. For both the $B_{N-2S}$ and $B_{CF-S}$ bus pads, the UPV values varied from 3 to 4.5 km/sec which indicates good quality of concrete. The lesser values in $B_{CF-S}$ are indicative of the scatter in the wave energy due to the presence of carbon fibers.

Based on the DT and NDT results, the CFRC bus pad is a conductive pavement likely to be effective in controlling the rate of crack initiation in the pavement. CFRC with a very low electrical resistivity can be used as a self-sensing construction material, able to sense and record internal deficiencies in the bus pad.

## Declaration of Competing Interest

The authors declare that they have no known competing financial interests or personal relationships that could have appeared to influence the work reported in this paper.

## Data Availability

Data will be made available on request.

## Acknowledgment

The authors acknowledge the financial support provided by Alberta Innovates. Involvement and guidance of Dr. Paolo Bomben is greatly acknowledged. Support received from CAMTEC research centre is also appreciated. Assistance from civil department's technical staff and co-op student Kara Labelle is greatly appreciated. Input from colleague Boyu Wang is appreciated.

## References

[1] Municipal Roads - The Canadian Infrastructure Report Card Available online: http://canadianinfrastructure.ca/en/municipal-roads.html (Accessed on 9 December 2020).
[2] Government of Canada, S.C. Commuting to Work during COVID-19 Available online: https://www150.statcan.gc.ca/n1/pub/45-28-0001/2020001/article/00069-eng.htm (Accessed on 4 January 2021).
[3] M. Tiznobaik, M.T. Bassuoni, A test protocol for evaluating absorption of joints in concrete pavements, J. Test. Eval. 46 (4) (2017) 1636–1649.
[4] H.J. Oh, Y.K. Cho, S.-M. Kim, Experimental evaluation of crack width movement of continuously reinforced concrete pavement under environmental load, Constr. Build. Mater. 137 (2017) 85–95, https://doi.org/10.1016/j.conbuildmat.2017.01.080.
[5] D.X. Xiao, Z. Wu, Longitudinal cracking of jointed plain concrete pavements in louisiana: field investigation and numerical simulation, Int. J. Pavement Res. Technol. 11 (2018) 417–426, https://doi.org/10.1016/j.ijprt.2018.07.004.
[6] J. Liu, D. Zhao, J. Shen, Y. Zhang, Comparative study on crack and factor of continuously reinforced concrete pavement in the tunnel and outside, Procedia - Soc. Behav. Sci. 96 (2013) 98–103, https://doi.org/10.1016/j.sbspro.2013.08.014.
[7] Caminos: Un Nuevo Enfoque Para La Gestión y Conservación de Redes Viales | Digital Repository | Economic Commission for Latin America and the Caribbean Available online: https://repositorio.cepal.org/handle/11362/30314 (accessed on 4 January 2021).
[8] M. Monazami, R. Gupta, Influence of Polypropylene, Carbon and Hybrid Coated Fiber on the Interfacial Microstructure Development of Cementitious, Compos. *Fibers* 9 (11) (2021) 65.
[9] S. Harzallah, M. Chabaat, M. Saidani, M. Moussaoui, Numerical investigation of the seismic vulnerability of bridge piers strengthened with steel fibre reinforced concrete (SFRC) and carbon fibre composites (CFC), Case Stud. Constr. Mater. 17 (2022), e01235.
[10] M. Monazami, R. Gupta, Effect of Curing Age on Pull-Out Response of Carbon, Steel, and Synthetic Fiber Embedded in Cementitious Mortar Matrix, J. Mater. Civ. Eng. 34 (10) (2022) 04022275.
[11] Y. Haddaji, H. Majdoubi, S. Mansouri, T.S. Alomayri, D. Allaoui, B. Manoun, H. Hannache, Microstructure and flexural performances of glass fibers reinforced phosphate sludge based geopolymers at elevated temperatures, Case Stud. Constr. Mater. 16 (2022), e00928.
[12] A.R. de Azevedo, M.T. Marvila, M.L.P. Antunes, E.C. Rangel, R. Fediuk, Technological perspective for use the natural pineapple fiber in mortar to repair structures, Waste Biomass-.-. Valoriz. 12 (9) (2021) 5131–5145.
[13] A.R. Azevedo, T.E. Lima, R.H. Reis, M.S. Oliveira, V.S. Candido, S.N. Monteiro, Guaruman fiber: A promising reinforcement for cement-based mortars, Case Stud. Constr. Mater. 16 (2022), e01029.
[14] D.Y. Yoo, N. Banthia, Mechanical and structural behaviors of ultra-high-performance fiber-reinforced concrete subjected to impact and blast, Constr. Build. Mater. 149 (2017) 416–431.
[15] Zhang, J., Wu, Z., Yu, H., Ma, H., & Da, B. (2022). Mesoscopic Modeling Approach and Application for Steel Fiber Reinforced Concrete under Dynamic Loading: A Review. Engineering.
[16] B.H. Oh, J.C. Kim, Y.C. Choi, Fracture Behavior of Concrete Members Reinforced with Structural Synthetic Fibers, Eng. Fract. Mech. 74 (2007) 243–257, https://doi.org/10.1016/j.engfracmech.2006.01.032.
[17] J. Blazy, R. Blazy, Polypropylene fiber reinforced concrete and its application in creating architectural forms of public spaces, Case Stud. Constr. Mater. 14 (2021), e00549.
[18] I. Hussain, B. Ali, T. Akhtar, M.S. Jameel, S.S. Raza, Comparison of mechanical properties of concrete and design thickness of pavement with different types of fiber-reinforcements (steel, glass, and polypropylene), Case Stud. Constr. Mater. 13 (2020), e00429.
[19] D. Akhmetov, S. Akhazhanov, A. Jetpisbayeva, Y. Pukharenko, Y. Root, Y. Utepov, A. Akhmetov, Effect of low-modulus polypropylene fiber on physical and mechanical properties of self-compacting concrete, Case Stud. Constr. Mater. 16 (2022), e00814.
[20] P. Müller, J. Novák, J. Holan, Destructive and non-destructive experimental investigation of polypropylene fibre reinforced concrete subjected to high temperature, J. Build. Eng. 26 (2019), 100906.
[21] Noushini, A.; Vessalas, K.; Arabian, G.; Samali, B. Drying Shrinkage Behaviour of Fibre Reinforced Concrete Incorporating Polyvinyl Alcohol Fibres and Fly Ash Available online: https://www.hindawi.com/journals/ace/2014/836173/ (accessed on 23 April 2020).
[22] D. Shen, Z. Feng, T. Zhang, X. Tang, G. Jiang, Estimating stress relaxation and cracking potential of high-strength concrete reinforced with polyvinyl alcohol fiber at early age, J. Mater. Civ. Eng. 34 (9) (2022) 04022223.
[23] Mechanical Properties of Geopolymer Concrete Containing Polyvinyl Alcohol Fiber Exposed to High Temperature, Constr. Build. Mater. 126 (2016) 381–387, https://doi.org/10.1016/j.conbuildmat.2016.09.001.
[24] S. Ahmad, A. Umar, Rheological and Mechanical Properties of Self-Compacting Concrete with Glass and Polyvinyl Alcohol Fibres, J. Build. Eng. 17 (2018) 65–74, https://doi.org/10.1016/j.jobe.2018.02.002.
[25] M. Karamloo, O. Afzali-Naniz, A. Doostmohamadi, Impact of using different amounts of polyolefin macro fibers on fracture behavior, size effect, and mechanical properties of self-compacting lightweight concrete, Constr. Build. Mater. 250 (2020), 118856.
[26] M.G. Alberti, A. Enfedaque, J.C. Gálvez, C. Álvarez, Using polyolefin fibers with moderate-strength concrete matrix to improve ductility, J. Mater. Civ. Eng. 31 (9) (2019) 04019170.
[27] Karahancer, B.; Morova, N.; Karahancer, S.; Eriskin, E.; Terzi, S.; Saltan, M. Utility of Aramid, Polyolefin and Polypropylene Combination in Hot Mix Asphalt as a Fiber Material. In Proceedings of the Advances in Environmental Vibration and Transportation Geodynamics; Tutumluer, E., Chen, X., Xiao, Y., Eds.; Springer: Singapore, 2020; pp. 915–922.
[28] P.B. Sakthivel, S. Govindasami, N. Suman, Flexural Performance of Hybrid Polypropylene–Polyolefin FRC Composites, Asian J. Civ. Eng. 20 (2019) 515–526, https://doi.org/10.1007/s42107-019-00120-6.
[29] T. Wongtanakitcharoen, A.E. Naaman, Unrestrained Early Age Shrinkage of Concrete with Polypropylene, PVA, and Carbon Fibers, Mater. Struct. 40 (2007) 289–300, https://doi.org/10.1617/s11527-006-9106-z.
[30] D.D.L. Chung, Cement Reinforced with Short Carbon Fibers: A Multifunctional Material, Compos. Part B: Eng. 31 (2000) 511–526, https://doi.org/10.1016/S1359-8368(99)00071-2.
[31] Nie, L.; Xu, J.; Luo, X.; Chen, H.; Chang, S.; Wang, T.; Liu, G. Study of Aramid and Carbon Fibers on the Tensile Properties of Early Strength Cement Mortar. IOP Conf. Ser.: Earth Environ. Sci. 2019, 267, 032009, doi:10.1088/1755–1315/267/3/032009.
[32] P. Nuaklong, A. Wongsa, K. Boonserm, C. Ngohpok, P. Jongvivatsakul, V. Sata, P. Chindaprasirt, Enhancement of mechanical properties of fly ash geopolymer containing fine recycled concrete aggregate with micro carbon fiber, J. Build. Eng. 41 (2021), 102403.

[33] M.N. Akhtar, J. Akhtar, O.H.A. Hattamleh, A.M. Halahla, Sustainable Fly Ash Based Roof Tiles with Waste Polythene Fibre: An Experimental Study, Open J. Civ. Eng. 06 (2016) 314, https://doi.org/10.4236/ojce.2016.62026.
[34] Mehvish, F., Ahmed, A., Saleem, M.M., & Saleem, M.A. (2020). Characterization of concrete incorporating waste polythene bags fibers. Pakistan Journal of Engineering and Applied Sciences.
[35] M. Zarei, A.A. Kordani, M. Khanjari, M. Zahedi, Evaluation of fracture resistance of asphalt concrete involving Calcium Lignosulfonate and Polyester fiber under freeze–thaw damage, Theor. Appl. Fract. Mech. 117 (2022), 103168.
[36] C. Gao, L. Huang, L. Yan, R. Jin, B. Kasal, Strength and Ductility Improvement of Recycled Aggregate Concrete by Polyester FRP-PVC Tube Confinement, Compos. Part B: Eng. 162 (2019) 178–197, https://doi.org/10.1016/j.compositesb.2018.10.102.
[37] Y. Gao, P. romero, H. Zhang, M. Huang, F. Lai, Unsaturated polyester resin concrete: a review, Constr. Build. Mater. 228 (2019), 116709, https://doi.org/10.1016/j.conbuildmat.2019.116709.
[38] S. Gupta, V.V.L.K. Rao, J. Sengupta, Evaluation of polyester fiber reinforced concrete for use in cement concrete pavement works, Road. Mater. Pavement Des. 9 (2008) 441–461, https://doi.org/10.1080/14680629.2008.9690127.
[39] B. Şimşek, T. Uygunoğlu, Thermal, electrical, mechanical and fluidity properties of polyester-reinforced concrete composites, Sādhanā 43 (2018) 57, https://doi.org/10.1007/s12046-018-0847-5.
[40] C. Maia Pederneiras, R. Veiga, J. de Brito, Impact resistance of rendering mortars with natural and textile-acrylic waste fibres, Fibers 10 (5) (2022) 44.
[41] C.B. Farinha, J. de Brito, R. Veiga, Incorporation of high contents of textile, acrylic and glass waste fibres in cement-based mortars' fresh, mechanical and deformability behaviour, Constr. Build. Mater. 303 (2021), 124424.
[42] M. Sappakittipakorn, P. Sukontasukkul, H. Higashiyama, P. Chindaprasirt, Properties of hooked end steel fiber reinforced acrylic modified concrete, Constr. Build. Mater. 186 (2018) 1247–1255.
[43] Y. Qin, M. Li, Y. Li, W. Ma, Z. Xu, J. Chai, H. Zhou, Effects of nylon fiber and nylon fiber fabric on the permeability of cracked concrete, Constr. Build. Mater. 274 (2021), 121786.
[44] M.A. Farooq, M. Fahad, B. Ali, M.H. El Ouni, A.B. Elhag, Influence of nylon fibers recycled from the scrap brushes on the properties of concrete: valorization of plastic waste in concrete, Case Stud. Constr. Mater. 16 (2022), e01089.
[45] S. Orasutthikul, D. Unno, H. Yokota, Effectiveness of recycled nylon fiber from waste fishing net with respect to fiber reinforced mortar, Constr. Build. Mater. 146 (2017) 594–602, https://doi.org/10.1016/j.conbuildmat.2017.04.134.
[46] Effects of Nylon Fibre and Concrete Strength on the Shrinkage and Fracture Behaviour of Fibre Reinforced Concrete | SpringerLink Available online: https://link.springer.com/chapter/10.1007/978-94-024-1194-2_22 (accessed on 24 April 2020).
[47] Giannopoulos, I.P.; Burgoyne, C.J. Stress Limits for Aramid Fibres. Proceedings of the Institution of Civil Engineers - Structures and Buildings 2009, 162, 221–232, doi:10.1680/stbu.2009.162.4.221.
[48] M.A. Ali, A.J. Majumdar, D.L. Rayment, Carbon fibre reinforcement of cement, Cem. Concr. Res. 2 (1972) 201–212, https://doi.org/10.1016/0008-8846(72)90042-7.
[49] P.-W. Chen, D.D.L. Chung, Low-drying-shrinkage concrete containing carbon fibers, Compos. Part B: Eng. 27 (1996) 269–274, https://doi.org/10.1016/1359-8368(95)00020-8.
[50] Abd Elrazek, M., Gamal, Y.A.S. (2021, July). The Reliable Concrete Compression Strength Assessment by SCHMIDT Hammer for Different Concrete Grades. In IOP Conference Series: Materials Science and Engineering (Vol. 1171, No. 1, p. 012004). IOP Publishing.
[51] S. Hedjazi, D. Castillo, Evaluation of elastic properties of fiber-reinforced concrete using fundamental resonance frequencies, Acids Mater. J. 118 (2021) 3.
[52] K. Nandhini, J. Karthikeyan, The early-age prediction of concrete strength using maturity models: a review, J. Build. Pathol. Rehabil. 6 (1) (2021) 1–10.
[53] Diaferio, M., Vitti, M., 2021. Correlation curves to characterize concrete strength by means of UPV tests. In Proceedings of 1st International Conference on Structural Damage Modelling and Assessment (pp. 209–218). Springer, Singapore.
[54] J.F. Scherr, C.U. Grosse, Delamination detection on a concrete bridge deck using impact echo scanning, Struct. Concr. 22 (2) (2021) 806–812.
[55] J. Helal, M. Sofi, P. Mendis, Non-destructive testing of concrete: a review of methods, Electron. J. Struct. Eng. 14 (1) (2015) 97–105.
[56] M. Monazami, R. Gupta, Investigation of mechanical behavior and fracture energy of fiber-reinforced concrete beams and panels, Cem. Concr. Compos. 133 (2022), 104656.
[57] ACI PRC-544.4–18: Guide to Design with Fiber-Reinforced Concrete Available online: https://www.concrete.org/store/productdetail.aspx?ItemID=544418&Language=English&Un its=US_AND_METRIC (Accessed on 26 October 2021).
[58] C01 Committee Test Method for Flow of Hydraulic Cement Mortar; ASTM International; C01 Committee Test Method for Compressive Strength of Hydraulic Cement Mortars (Using 2-in. or [50 mm] Cube Specimens); ASTM International;.
[59] ASTM C109/C109–05 Standard Test Method for Compressive Strength of Hydraulic Cement Mortars (Using 2-in. or [50 mm] Cube Specimens. ASTM C109/C109–05. 2008: Annual book of ASTM Standards.
[60] ASTM C307 - 18 Standard Test Method for Tensile Strength of Chemical-Resistant Mortar, Grouts, and Monolithic Surfacings Available online: https://www.astm.org/Standards/C307.htm (Accessed on 1 November 2021).
[61] C09 Committee Test Method for Flexural Strength of Concrete (Using Simple Beam With Center-Point Loading); ASTM International;.
[62] ASTM C143 / C143M - 20 Standard Test Method for Slump of Hydraulic-Cement Concrete Available online: https://www.astm.org/Standards/C143 (Accessed on 7 April 2021).
[63] C09 Committee Test Method for Compressive Strength of Cylindrical Concrete Specimens; ASTM International;.
[64] C09 Committee Test Method for Flexural Toughness of Fiber Reinforced Concrete (Using Centrally Loaded Round Panel); ASTM International;.
[65] CSA CAN/CSA-A300–13-Cementitious Materials Compendium (2009).
[66] B.C. Transit - Planning Standards and Guidelines | Transit Future | BC Transit Available online: https://bctransit.com/kamloops/transit-future/corporate-infrastructure-initiatives/design-guidelines (accessed on 7 April 2021).
[67] ASTM C231 / C231M-17a, Standard Test Method for Air Content of Freshly Mixed Concrete by the Pressure Method, ASTM International, West Conshohocken, PA, 2017, www.astm.org.
[68] D.G. Goulias, H. Kim, C.W. Schwartz, Evaluation of in situ pavement material properties and behavior through field instrumentation and load testing, J. Transp. Eng. 137 (7) (2011) 466–473.
[69] D. Merkle, A. Reiterer, Evaluation of thermography-based automated delamination and cavity detection in concrete bridges, in: Automated Visual Inspection and Machine Vision IV, Vol. 11787, SPIE, 2021, pp. 38–49.
[70] Agilent | Agilent History Timeline -, 2000s. Available online: https://www.agilent.com/about/companyinfo/history/timeline_2000s.html (Accessed on 1 November 2021).
[71] D. Breysse, J.L. Martínez-Fernández, Assessing concrete strength with rebound hammer: review of key issues and ideas for more reliable conclusions, Mater. Struct. 47 (2014) 1589–1604.
[72] ASTM C805 / C805M - 18 Standard Test Method for Rebound Number of Hardened Concrete Available online: https://www.astm.org/Standards/C805.htm (accessed on 1 November 2021).
[73] A. Sassani, A. Arabzadeh, H. Ceylan, S. Kim, S.S. Sadati, K. Gopalakrishnan, H. Abdualla, Carbon fiber-based electrically conductive concrete for salt-free deicing of pavements, J. Clean. Prod. 203 (2018) 799–809.
[74] C. Li, H. Ge, D. Sun, X. Zhou, Novel conductive wearing course using a graphite, carbon fiber, and epoxy resin mixture for active de-icing of asphalt concrete pavement, Mater. Struct. 54 (1) (2021) 1–17.
[75] A. Sassani, A. Arabzadeh, H. Ceylan, S. Kim, S.S. Sadati, K. Gopalakrishnan, H. Abdualla, Carbon fiber-based electrically conductive concrete for salt-free deicing of pavements, J. Clean. Prod. 203 (2018) 799–809.

[76] C09 Committee Test Method for Pulse Velocity Through Concrete; ASTM International;.
[77] A. Adesina, A. Bastani, J.Z. Heydariha, S. Das, D. Lawn, Performance of basalt fibre-reinforced concrete for pavement and flooring applications, Innov. Infrastruct. Solut. 5 (3) (2020) 1–10.
[78] N.I. Zulkifli, A. Alisibramulisi, N. Saari, R. Hassan, E. Shaffie, N.M. Bhkari, M.N.M. Sidek, Experimental investigation of ultrasonic pulse velocity (UPV) test specimen in assessing the strength of steel fiber reinforced concrete structure, J. Adv. Ind. Technol. Appl. 2 (2) (2021) 34–41.